VISER

Research Article   **Open Access**

B, N-Co-doped Carbon Tubes with P Encapsulated in 3D Graphene Aerogel for High-stable Lithium-ion Batteries

Fengfeng XU[†], Jian LIN[†], Cuiyan TONG*, Haizhu SUN*

National & Local United Engineering Laboratory for Power Battery, College of Chemistry, Northeast Normal University, Changchun 130024, China

***Corresponding Author:** Haizhu SUN, E-mail: sunhz335@nenu.edu.cn; Cuiyan TONG, E-mail: tongcy959@nenu.edu.cn.*

Abstract:

Li-related anodes with stable ability and excellent rate performance are urgently being pursued to overcome the slow kinetic of current lithium ion storage devices. In this work, an annealing-hydrothermal method is developed to fabricate the anode of a three-dimension nano-construction with robust charge transfer networks, which is composed of elements B, N co-doped carbon tube (BN-CT) as the carrier of red phosphorous to (3D BN-CT@P). Then, 3D BN-CT@P is embedded in the graphene aerogel network to obtain 3D BN-CT@P@GA). Impressively, the 3D BN-CT@P@GA shows high capacity and good cycle stability in the potential rage of 0.01-2.5V. Especially, the discharge capacity is ~800 mAh g^{-1} at 500 mA g^{-1} after 500 cycles when evaluated as anode materials for lithium-ion batteries (LIBs). The improved electrochemical performances result from the unique structure of the 3D BN-CT@P@GA. With the hetero atoms doping, the active P can load up to the BN-CT, which can realize the high capacity as well as the low potential for the anode. At the same time, the graphene aerogel network provides the protection for the BN-CT@P species and good conductivity to enhance ion diffusion. This work fundamentally presents an effective structural engineering way for improving the performance of P-based anodes for advanced LIBs.

Keywords: red phosphorus; nanostructure; anode material; lithium-ion batteries

1 Introduction

Environmental issues and the rapid development of electronic products make it urgent to improve the performance of energy storage devices. As one of the most promising energy storage devices, lithium-ion battery (LIBs) has attracted lots of interests because of their low cost and high energy density [1-3]. Graphite possesses a theoretical capacity of 372 mAh g^{-1} which is used for commercial LIB anode materials [4]. However, the higher capacity is indispensable for the high energy storage system. For anode electrodes, higher theory capacity and the lower potential are two important factors for the high energy density. In addition, it is worth noting that the lower potential in anode will involve in the safety hazard because the approach of Li-formation potential (0 V). Therefore, it is significant to develop novel kind of anode materials.

Red phosphorus (P) has aroused extensive attention in LIBs due to its high theoretical specific capacity of 2596 mAh g^{-1} [5-6]. Moreover, red phosphorus shows the relatively low and safe working potential (~0.7 V in average Vs. Li$^+$/Li) which has the capacity to be the high energy storage materials [7]. However, the biggest limit for red phosphorus is its tremendous volume expansion during the process of lithiation-delithiation reaction [8-9]. Besides, low conductivity is another impedance to be addressed especially under high-rate conditions [10-11].

To solve these problems, nano-sized red phosphorus particles and their composites with other high conductivity materials (e.g., carbonaceous materials) are supposed to be the most effective approaches to enhance the conductivity. For instance, Liu et al encapsulated nanosized red phosphorus into hierarchical porous carbon nanospheres through a vaporization−condensation process, achieving a high capacity of 2463.8 mAh g^{-1} at 0.1 A g^{-1} and a decent rate performance of 842.2mAh g^{-1} at 10 A g^{-1}. Jiao et al reported synthesis of red phosphorus/crumpled nitrogen-doped graphene nanocomposites through a ball-milling process with a high capacity of 2522.6 mAh g^{-1} at 130 mA g^{-1}, a great cyclability of 1470.1 mAh g^{-1} at 1300 mA g^{-1} for 300 cycles as well as a satisfactory rate capacity of 1340.5 mAh g^{-1} at 3900 mA g^{-1} [12-13].

Herein, B, N co-doped carbon tube with P encapsuled into the 3D graphene (GO) aerogel network

(3D BN-CT@P@GA) was fabricated. Taking advantages of the BN-doped carbon tube as the P carrier (BN-CT@P), the BN-CT@P was well composited with GA. The B, N-doped hollow carbon tube increased the specific surface area, shortened the ion transmission path, and improved the Li$^+$ kinetics. P source was further stabilized after composited with GO in which it not only tightly contacted on the BN-CT but also is protected by rGO layer. As a result, the 3D BN-CT@P@GA possessed excellent cycle stability that delivered reversible $\sim$750 mAh g^{-1} at 500 mA g^{-1} for 500 cycles.

2 Experimental section

Briefly, urea, polyethylene glycol (PEO, Mw = 4000 M), boric acid and red phosphorus were purchased from Aladdin. The hydrochloric acid, ethanediamine were purchased from Macklin. All the medicines were use directly without further purification.

2.1 Synthesis of BN-CT

Briefly, 5.0 g urea and 0.5 g PEO were added into deionized water (50 mL) and stirred for 10 min at a proper rate. After that, 0.5 g boric acid was supplied in the beaker. The pH value of the precursor solution was tuned to $\sim$3 with hydrochloric acid and stirred for another 30 min. Next, the precursor solution was transferred into the oven at the 120°C to finish the evaporation and crosslinking. Then, the cross-linked white solid was transferred into the porcelain with the small window at the temperature 600°C in the nitrogen gas (5°C min^{-1}). Finally, the BN-carbon tube (BN-CT) were prepared.

2.2 Synthesis of BN-CT@P

The BN-CT@P was prepared by vacuum evaporation deposition method. Typically, 0.02 g BN-CT and 0.05 g red phosphorus were mixed together and loaded into the glass tube with the diameter of 0.6 cm in argon atmosphere and annealed at 460℃ for 3 h and provided cooling time for 20 h for phase conversion. Finally, the composite was washed using CS$_2$ solvent to form a pure surface.

2.3 Synthesis of 3D BN-CT@P@GA

0.2 g BN-CT@P, 0.05 g GO and 60 μL ethanediamine were dissolved into 10 mL water in 20 mL capacity glass vial. Then, the vial was transferred into oven and reacted for 8 h at 180 ℃.

2.4 Materials characterizations

The phase and morphology of the prepared products were characterized by using an X-ray diffractometer (PXRD, Smartlab) and a scanning electron microscopy (10 kV, FESEM, HITACHI SU8010).

2.5 Electrochemical measurements

The electrochemical capacities were evaluated by assembled coin-type lithium ion cell. Metallic lithium foil was used as the counter electrode and a polypropylene microporous membrane (Celgard 2400) was used as the separator. The BN-CT@P@GA anodes were coated on Cu foil with the staff mass ratio of 8:1:1 (BN-CT@P@GA powder/acetylene black/ Super P). The final specific capacity was calculated based on the quality of active materials on copper ($\sim$ 1 mg). After drying for 12 h at the temperature 80°C in the vacuum oven, the final electrodes were obtained using a compact and precision disc cutter (MSK-T-10, MTI Corporation). The electrolyte was composed of 1 M LiPF6-ethylene carbonate (EC)- dimethyl carbonate (DMC)-ethylmethyl carbonate (EMC) (1 : 1 : 1 by volume). Coin cells were assembled using a compact hydraulic crimping machine (MSK-110, MTI Corporation) in an argon-filled glove-box (Universal 2400/750/900, MIKROUNA) with oxygen and water value lower than 0.1 ppm. The galvanostatic charge–discharge (GCD) tests of BN-CT@P@GA were carried out using a battery testing system LAND CT2001 (Wuhan LAND electronics, China) with a cutoff voltage range from 0.01 V to 2.5 V (vs. Li$^+$/Li). For the electrochemical impedance spectroscopy (EIS) measurements, the frequency ranged from 0.01 kHz to 100 Hz.

3 Results and discussion

Figure 1 illustrates the synthesis process of 3D BN-CT@P@GA. The BN-CT is prepared after heating. In the typical process, the assembled carbon tubes as the P carrier derive from the PEO and the heteroatoms originate from boric acid and itself. As known, heteroatoms such as N, B and P can adjust local charge redistribution in carbon-base materials, which can form the center of negative charge and hence bring in the pseudo capacitance effect to increases the capacity. Next, P species are loaded on BN-CT by using the evaporation-deposition method in the inert protect gas. After that, in order to protect the active materials P and provide good electrical conductivity, reductive graphene aerogel network is designed with hydrothermal and freeze drying to encapsule the BN-CT@P. The resultant BN-CT@P@GA shows the freestanding feature and ensures the structural integrity of BN-CT@P.
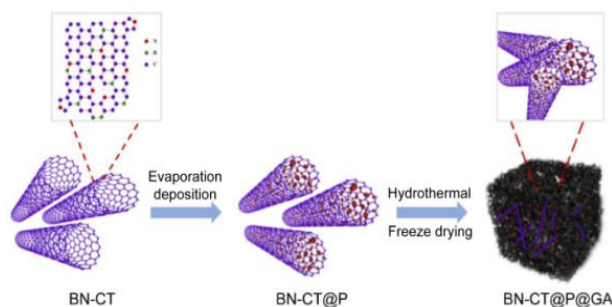

Figure 1 The synthesis procedure of the 3D BN-CT@P@GA
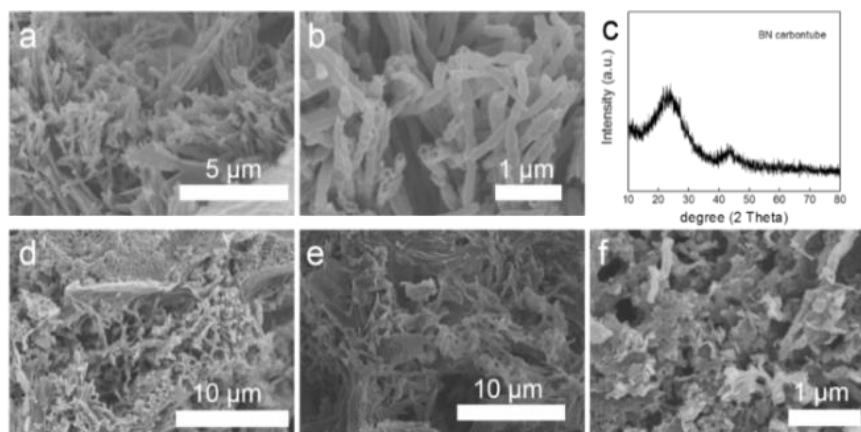
Figure 2   SEM images of BN-CT under different annealing conditions: (a-b) the resulted BN-CT at 850°C, namely, BN-CT-850, (c) XRD pattern of BN-CT-850, (d) BN-CT-700, (e) BN-CT-900, (f) BN-CT-1000

The BN-CT is obtained by simple and scalable annealing method. Figure 2 shows SEM images prepared at different temperatures (BN-CT-X, X represents the temperature). The uniform hollow BN carbon tubes (BN-CT) were successfully synthesized after optimized the temperature to 850°C (BN-CT-850). The XRD pattern shows two diffraction peaks at approximately 23° and 43°, which corresponds to (002) and (100) lattice planes, respectively (Figure 2c). This result indicates that the BN-CT-850 is amorphous [14]. From HRTEM (Figure S1), the crystalline of the carbon tube is confirmed by the obvious (002) lattice. It is worth mentioning that the temperature is a crucial factor for the formation of BN-CT. When precursor is reacted at 700°C, only incomplete carbon tubes are formed and separate tiny particles are appeared (Figure 2d). When the temperature increases to 900°C, carbon tubes partly disappear along with the formation of the ultra-thin nanosheets (Figure 2e). When continue to heat up to 1000°C, the carbon tubes link up and turn into the carbonsheets (Figure 2f). This means the BN-CT nanostructure is obtained only at the proper temperature of 850°C.
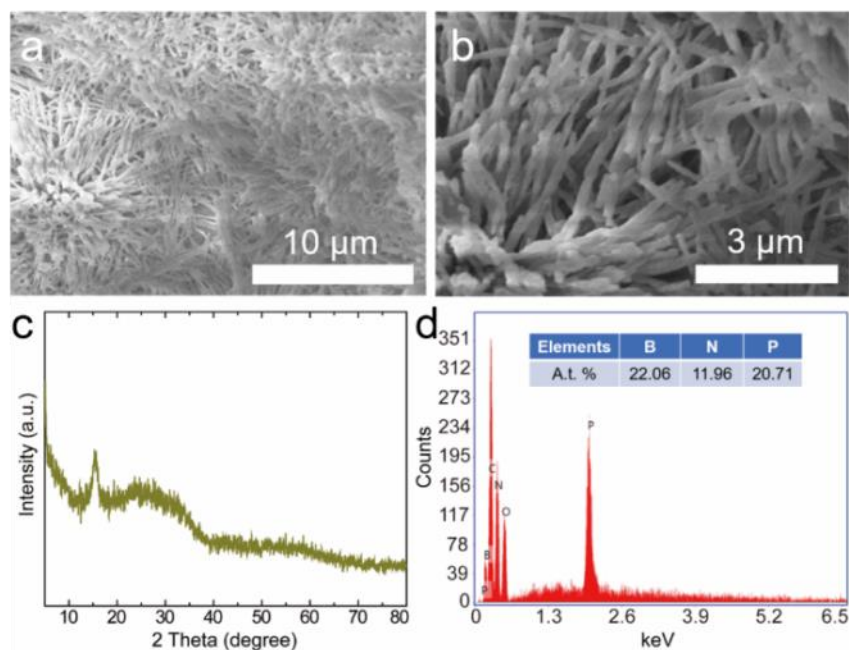

Figure 3   (a-b) The SEM images of BN-CT@P with scales of 10 μm and 3 μm. (c) The XRD pattern of BN-CT@P. (d) The energy dispersive spectrum (EDS) of BN-CT@P, confirming the formation of BN-CT@P

The SEM images of phosphatized BN-CT (BN-CT@P) (Figure 3a-b) exhibit the initial BN carbon tubes morphology, indicating the structure isn't damaged during the phosphating process. As confirmed in XRD pattern, three broadened diffraction peaks located at 13-16°, 25-38°, and 47-65° are consistent with the reported phosphorus-related works (Figure 3c) [15]. In addition, the energy dispersive spectrum (EDS) image identifies that the B, N and P species are uniformly distributed with the content of 22.06 %, 11.96 % and 20.71 %, respectively (Figure 3d and the inset Table). The XPS full spectrum also shows B and N successfully doped in carbon tube (Figure S2).
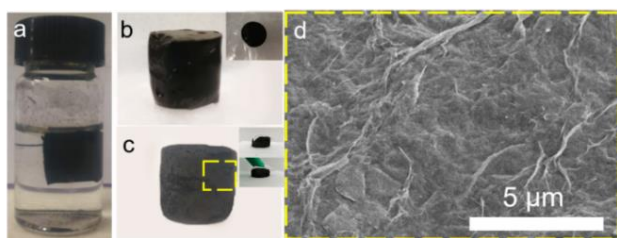
Figure 4 (a-b) Photos of BN-CT@P@GA after hydrothermal reaction. (c) The BN-CT@P@GA exhibit its toughness after free-dried process when given the tough press (insets). (d) The SEM image of BN-CT@P@GA, indicating that the rGO nanosheets cover the surface and protect the structural integrity of BN-CT@P

During hydrothermal reaction with the proper amount precursors, the assembled 3D BN-CT@P-graphene aerogel is prepared (Figure 4a-b) with the dimeter of 1.7 cm (inset in Figure 4b). The 3D structure is well reserved and shows the toughness after free-dried process. Figure 4d (the microscopic amplification of BN-CT@P-graphene aerogel) shows the thin rGO nanosheets cover on the surface of BN-CT@P and protect the structure integrity, which alleviate the structure pulverization and deactivation of the active material caused by volume expansion. Especially, when given strong press ($\sim$1 N cm^{-2}) to the BN-CT@P@GA, it still maintains the structure integrity as shown inset of Figure 4c.
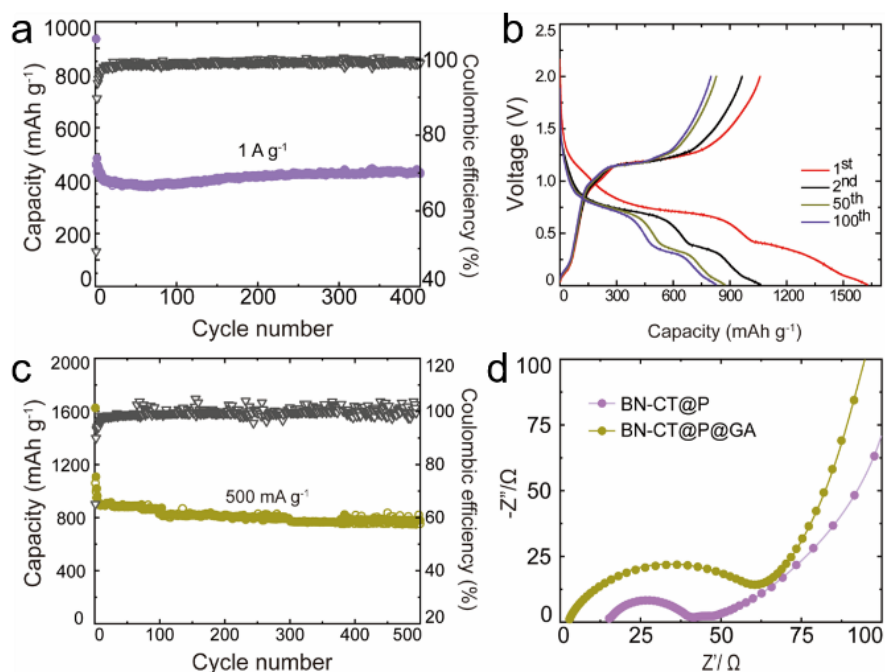

Figure 5 (a) The cyclic performance chart of BN-CT at 1 A g-1. (b) GCD curves for the different cycles. (c) The cyclic performance chart of BN-CT@P@GA at 500 mA g^{-1}. (d) The EIS of BN-CT@P and BN-CT@P@GA

The electrochemical performance of the BN-CT was evaluated at 1 A g^{-1}. The BN-CT anode delivers a better cycling and maintains a stability capacity of 430 mAh g^{-1} after 400 cycles with an average capacity fading only 0.075% per cycle (Figure 5a). It keeps the nature stability of carbon-based materials [16-18]. After loading P and composited with GO, the capacity shows obvious enhancement (Figure 5b). There is a distinct discharge platform $\sim$0.7 V that indicates the capacity contribution of P species [19]. Favorable curve repeatability after 100 cycles shows the BN-CT@P@GA can deliver the reversible performance resulting from its structure.

Moreover, the prolonged cycling performance of BN-CT@P@GA at 500 mA g^{-1} is detected. The initial Coulombic efficiency (ICE) is 65% which is mostly attributed to the formation of SEI from the side reactions of electrolyte on the BN-CT@P@GA surface [20-21]. After the formation of SEI, the maintained capacity $\sim$800

mAh g^{-1} is delivered with no fluctuation (Figure 5c). These results demonstrate that fabrication of BN-CT@P@GA composite is an effective strategy to fix the P species in the skeleton and makes it possible to apply in the energy storage system. The EIS of BN-CT@P and BN-CT@P@GA are exhibited in Figure 5d. Both of them are composed of the semicircle in the high-frequency areas and a liner in the low-frequency areas. The high-frequency area is related to the internal resistance (including separator, electrode/electrolyte and the electrical contact). From Figure 5d, the BN-CT@P shows the smaller internal resistance, indicating the better electron transportation. However, steeper slope at the low-frequency of the BN-CT@P@GA confirms the higher Li$^+$ diffusivity on the electrolyte-electrode interface. It shows that BN-CT@P@GA material as LIB anode has high rate performance. Figure 6 shows the morphology of BN-CT@P@GA after disassemble the

battery. The BN-CT@P still encapsulate in the graphene network and the whole structure maintains integrity, indicating a highly stable constructing for lithium ions.
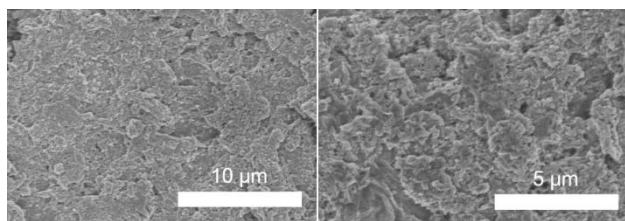

Figure 6 The SEM images of BN-CT@P@GA after 200 cycles at 500 mA g^{-1}

4 Conclusion

In summary, an interesting 3D BN-CT@P@GA skeleton is achieved successfully to protect the active mass P from volume expansion pulverization deactivation. Meantime, a new route to fabricate the double protected network of P is developed (BN-CT carrier effect and graphene aerogel reinforcement effect). Benefiting from the open and connected space of carbon skeleton, the fabricated 3D BN-CT@P@GA sample shows an improved structural stability during the charge-discharge process. As the anode of LIBs, it can deliver a high reversible capacity ~800 mAh g^{-1} at 500 mA g^{-1} and excellent cycling stability for 500 cycles. Therefore, this work may offer a novel strategy for rational design of high-performance electrode materials for Li$^+$-based energy storage devices.

References

[1] Jiang Y, Wen J, Ding Z, et al. Li$^+$ storage properties of SiO$_2$@C core-shell submicrosphere and its hollow counterpart synthesized by molecular self-assembly in wet-chemistry condition as anodes for LIBs. Journal of Alloys and Compounds, 2021; 861.

[2] Lopez J, Gonzalez R, Ayala J, et al. Centrifugally spun TiO$_2$/C composite fibers prepared from TiS$_2$/PAN precursor fibers as binder-free anodes for LIBS. Journal of Physics and Chemistry of Solids, 2021; 149.

[3] Zhang X, Qiu Y, Cheng F, et al. Realization of a High-Voltage and High-Rate Nickel-Rich NCM Cathode Material for LIBs by Co and Ti Dual Modification. ACS Appl Mater Interfaces, 2021, 13 (15): 17707-17716.

[4] Rabiei Baboukani A, Khakpour I, Adelowo E, et al. High-performance red phosphorus-sulfurized polyacrylonitrile composite by electrostatic spray deposition for lithium-ion batteries. Electrochimica Acta, 2020; 345.

[5] Liang S, Pei X, Jiang W, et al. Free standing dual-network red phosphorus@porous multichannel carbon nanofifibers/carbon nanotubes as a stable anode for lithium-ion batteries. Electrochimica Acta, 2019, 322: 134696.

[6] Xue J, Wang D, Xia X, et al. Confined red phosphorus in N-doped hierarchically porous carbon for lithium ion batteries with enhanced rate capability and cycle stability. Microporous and Mesoporous Materials, 2020, 305.

[7] Wu K, Xu G, Pan D, et al. Red phosphorus confined in MOF-derived N-doped carbon-based composite polyhedrons on carbon nanotubes for high-areal-capacity lithium storage. Chemical Engineering Journal, 2020, 385: 123456.

[8] Chen X, Qiu J, Wang Y, et al. A stable polypyridinopyridine–red phosphorus composite as a superior anode material for long-cycle lifetime lithium-ion batteries. New Journal of Chemistry, 2019, 43 (16): 6197-6204.

[9] Yan Y, Xu H, Peng C, et al. 3D phosphorus-carbon electrode with aligned nanochannels promise high-areal-capacity and cyclability in lithium-ion battery. Applied Surface Science, 2019, 489: 734-740.

[10] Zhang Y, Sun L, Zhao X, et al. Construction of Sn-P-graphene microstructure with Sn-C and P-C co-bonding as anodes for lithium-ion batteries. Chem Commun (Camb), 2020, 56 (72): 10572-10575.

[11] Liu H, Zhang S, Zhu Q, et al. Fluffy carbon-coated red phosphorus as a highly stable and high-rate anode for lithium-ion batteries. Journal of Materials Chemistry A, 2019, 7 (18): 11205-11213.

[12] Liu B, Zhang Q, Li L, et al. Encapsulating Red Phosphorus in Ultralarge Pore Volume Hierarchical Porous Carbon Nanospheres for Lithium/Sodium-Ion Half/Full Batteries. ACS Nano, 2019, 13 (11): 13513-13523.

[13] Jiao X, Liu Y, Li T, et al. Crumpled Nitrogen-Doped Graphene-Wrapped Phosphorus Composite as a Promising Anode for Lithium-Ion Batteries. ACS Appl Mater Interfaces, 2019, 11 (34): 30858-30864.

[14] Yang H, Zhou J, Wang M, et al. From basil seed to flexible supercapacitors: Green synthesis of heteroatom‐enriched porous carbon by self‐gelation strategy. International Journal of Energy Research, 2020, 44 (6):

4449-4463.

[15] Chang W. C, Tseng K. W, Tuan H. Y. Solution Synthesis of Iodine-Doped Red Phosphorus Nanoparticles for Lithium-Ion Battery Anodes. Nano Lett, 2017, 17(2): 1240-1247.

[16] Kong W, Yu J, Shi X, et al. Encapsulated Red Phosphorus in rGO-C$_3$N$_4$ Architecture as Extending-Life Anode Materials for Lithium-Ion Batteries. Journal of The Electrochemical Society, 2020, 167 (6).

[17] Shen J, Wang Y, Yao Y, et al. Flexible Free-Standing Hierarchical Carbon-Coated CoP$_2$ Nanosheets for High-Performance Lithium-Ion Batteries. ACS Applied Energy Materials, 2018; 1 (12), 7253-7262.

[18] Wang L, Ju J, Deng N, et al. Embedding red phosphorus in hierarchical porous carbon nanofibers as anodes for lithium-ion battery. Materials Letters, 2019, 240: 39-43.

[19] Wang T, Wei S, Villegas Salvatierra R, et al. Tip-Sonicated Red Phosphorus-Graphene Nanoribbon Composite for Full Lithium-Ion Batteries. ACS Appl Mater Interfaces, 2018, 10 (45): 38936-38943.

[20] Jiao X, Liu Y, Li B, et al. Amorphous phosphorus-carbon nanotube hybrid anode with ultralong cycle life and high-rate capability for lithium-ion batteries. Carbon, 2019, 148: 518-524.

[21] Zhang S, Liu C, Wang H, et al. A Covalent P-C Bond Stabilizes Red Phosphorus in an Engineered Carbon Host for High-Performance Lithium-Ion Battery Anodes. ACS Nano, 2021, 15 (2): 3365-3375.